Normalized Reflectivity in Reverse Time Migration

André Bulcão, Gustavo Catão Alves & Djalma Manoel Soares Filho, CENPES/PETROBRAS, Brazil

Abstract

Reverse Time Migration has recently gained much attention as a viable and accurate technique for imaging reflectors, especially in complex geologies. However, reflection amplitudes in RTM are problematic and limit its applications when correct reflectivity is necessary.

In this work, normalized reflectivity amplitudes for reflectors in Reverse Time Migration are achieved when the amplitude matrix used for the excitation time image condition is applied as a normalization factor to the migrated image.

The amplitude matrix acts as a weighing factor that takes into account the illumination of the target reflector, giving more accurate results for the reflection coefficient.

Results are shown for a simple 2D horizontal model and for 2D horizontal model with a diving reflector. In both cases, a reflection coefficient is obtained that closely matches the theoretical trend.

A wave separation technique applied for increasing the amplitude accuracy is also discussed (Bulcão et al 2007), despite the marginal gains.

Introduction

Reverse Time Migration is an efficient imaging technique that uses a wavefield extrapolation approach in order to correctly position reflectors in a seismic image. Because it is based on the complete wave equation, it offers advantages in comparison to ray tracing approaches, making it suitable for application in geologically complex areas, such as subsalt and sub basalt fields (Sava and Hill, 2009).

Although RTM has been proposed almost thirty years ago (Baysal, 1983), it is a much more computationally intensive technique than ray based methods, making it a costlier choice in processing. However, recent advances in computational power, and others hardware accelerators - for example - the use of GPUs (Graphics Processing Units), have made RTM feasible in seismic imaging.

One of the main concerns in RTM is the correct output of reflection coefficients (Zhang et al, 2007), which are necessary for many applications, such as AVA analyses. Although traditional RTM does not give true amplitudes, many solutions have been proposed in the literature to correct this. For example, Chattopadhyay and McMechan (2008) propose that true amplitude can be estimated by normalization of a crosscorrelation image by source illumination or by receiver/source-wavefield amplitude ratio. Another approach (Silva et al, 2010) involves substituting the two way wave equation with a non-reflective wave equation during depropagation.

The methodology proposed here is based on the normalization of the migrated image by the maximum amplitude matrix obtained during the propagation of the source wavefield. In other words, the amplitude matrix of the excitation time imaging condition is used (Loewenthal and Hu, 1991).

Also, a wave separation technique was employed to further enhance the relative accuracy of the reflection coefficient obtained. This was based on previous work by Bulcão *et al* (2007), but uses an angle dependant wave separation to account for different incident angles.

Methodology

Wavefield extrapolation to generate the synthetic seismograms was based on the widely used staggered finite differences, with a 4^{th} order in space and 2^{nd} order in time elastic operator (Levander, 1988). The use of the elastic operator during modeling allows the theoretical reflection coefficients to be estimated from Zoeppritz equations.

The P-wave seismogram obtained in the previous step, using the divergent as a separation scheme, was used as input for the Acoustic Reverse Time Migration.

Although the two-way acoustic wave equation was employed to extrapolate the source and receiver wavefields, a separation scheme could be applied to diminish the reflection that occurs when the wavefields reaches a layer with high impedance contrast, generating a low frequency noise (Bulcão, 2007).

A more sophisticated approach adopted the normal incidence of the wavefront, instead of separating the wavefield in only downgoing and upgoing directions. The incident of the wavefront was estimated using the gradient of the travel time matrix.

The normalized excitation time imaging condition used can be summarized according to equation 1 (Chattopadhyay and McMechan, 2008).

$$I = \frac{U(t = t_{TTM})}{D_{\max}(t = t_{TTM})}, \quad (1)$$

where $U(t=t_{TTM})$ is the upgoing (receiver) wavefield at the time of maximum amplitude, and $D_{max}(t=t_{TTM})$ is the downgoing (source) wavefield recorded at the same time.

In the conventional case, traditional excitation time imaging condition, the downgoing wavefield factor is dropped.

Results

The proposed methodology was applied to two velocity models. Figure 1 shows the first model, with constant horizontal layers and velocities that increase with depth. The model is 5120 m wide and 3200 m deep.

A synthetic seismogram (Figure 2) was obtained for a single shot at coordinates x=2560 m and z=5 m. The seismogram was modeled using the full elastic wave equation. Receivers were placed at every surface position and total recording time was 4 seconds, with 0.004 s interval. The grid spacing between receivers was 5 meters. The direct wave was removed and a damping zone applied to the sides, in order to attenuate artifacts in the migrated image. Although the seismogram was modeled with an elastic operator, only the pressure field (P-wave) was recorded.

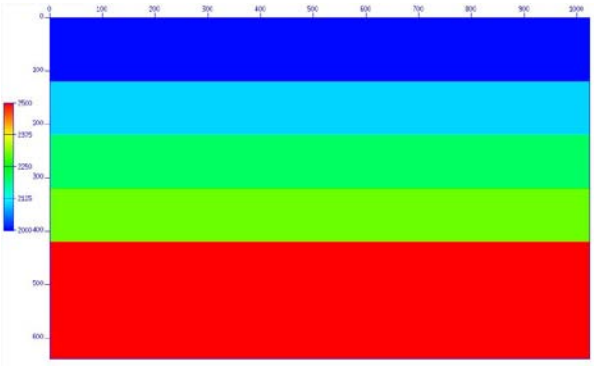

Figure 1 - Velocity model with horizontal layers.

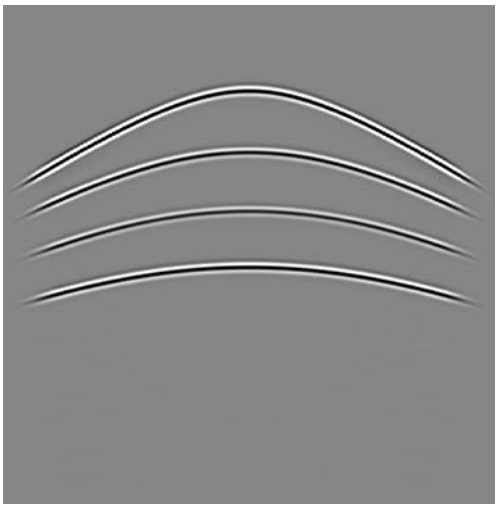

Figure 2 - Seismogram for the model with horizontal layers.

Reverse Time Migration was performed applying an acoustic two way wave equation with constant density. Two different excitation time imaging conditions (ETI) were employed, the conventional one and the directional one, as explained in the methodology. The migrated images for the conventional and directional cases are shown in figures 3 and 4, respectively.

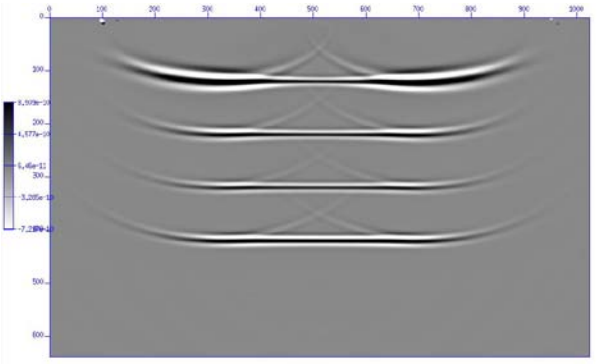

Figure 3 - RTM image for the conventional wavefield propagator for the horizontal model.

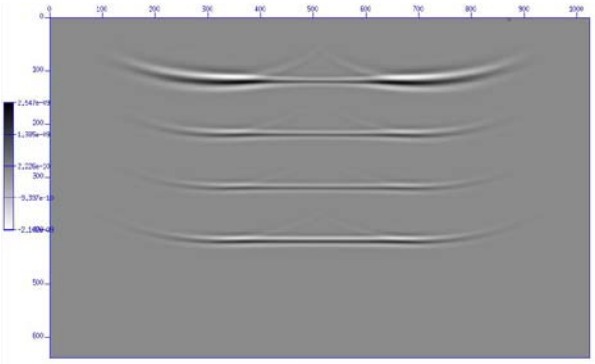

Figure 4 - RTM image for the directional wavefield propagator for the horizontal model.

For longer offsets the migrated images, figures 3 and 4, show interference in the measured amplitudes caused by discontinuity in the receiver data and also due to overlapping of the reflected and refracted waves, this effect is less pronounce in the case that uses the directional separation (figure 4).

The maximum available incident angle on the reflector can be increased by extending the velocity model and receiver coverage. However the overlapping of the reflected and head waves is related to properties and geometry of the model. The noise caused by the overlapping limited the region in which our analysis was performed.

Figures 5 through 8 show the scaled depth image amplitudes, using the normal incident value, for reflectors 1 through 4, respectively. In addition to the theoretical reflection coefficients, each graph shows the coefficient obtained for the conventional and directional cases, with and without normalization. In each case, the vertical line shows the maximum incident angle for receiver coverage.

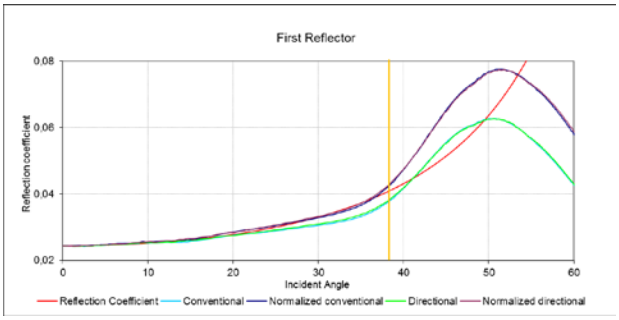

Figure 5 - Measured and theoretical reflection coefficient for the 1st reflector in the horizontal model.

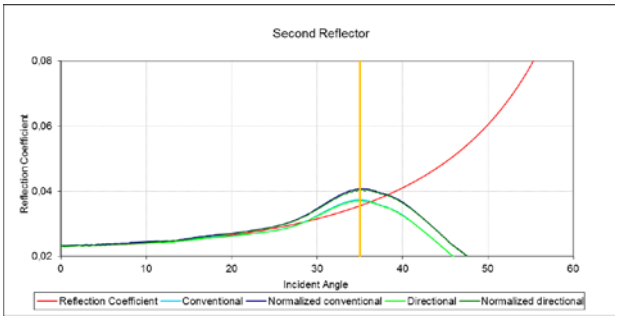

Figure 6 - Measured and theoretical reflection coefficient for the 2nd reflector in the horizontal model.

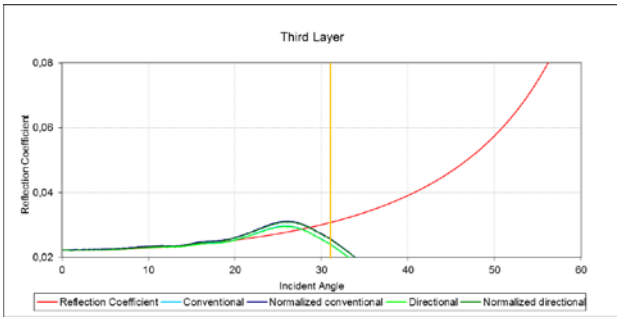

Figure 7 - Measured and theoretical reflection coefficient for the 3rd reflector in the horizontal model.

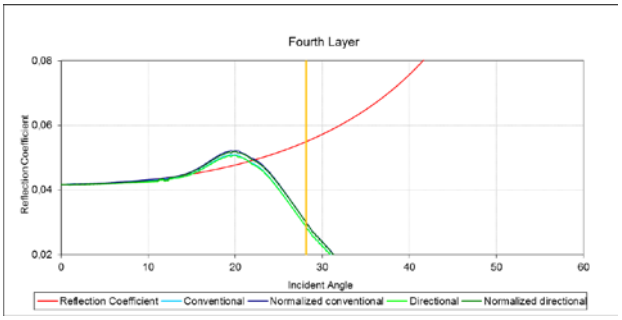

Figure 8 - Measured and theoretical reflection coefficient for the 4th reflector in the horizontal model.

All graphs show an improvement on following the trend of the reflection coefficients when the normalization factor was applied. For the first layer, the scaled measured reflectivity was equal to the theoretical one, up to the maximum receiver coverage. However, the overlapping refracted wave affected the lower layers at angles smaller than the maximum receiver coverage. The application of the wave separation method did not show significant improvements.

The second model, shown in Figure 9, adds a dipping layer beneath the first two reflectors of the preceding model. The aim was to enhance the effectiveness of the directional wave separation in the reflection coefficient trend. The migrated sections for the conventional and directional schemes are presented in figures 10 and 11, respectively.

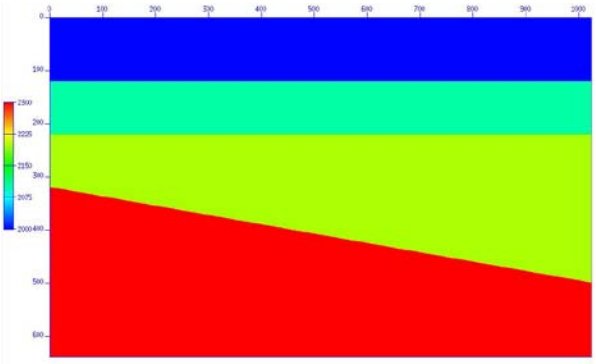

Figure 9 - Velocity model with dipping reflector.

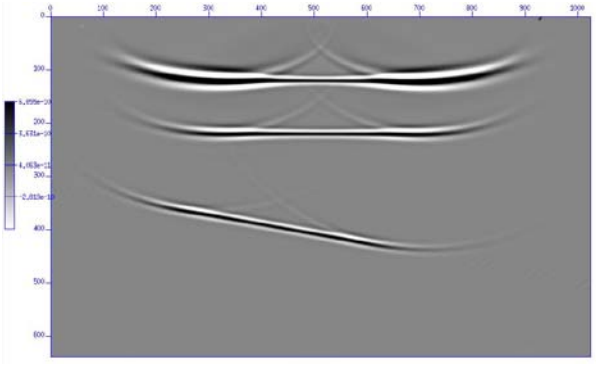

Figure 10 - RTM image for the conventional wavefield propagator for the dipping reflector model.

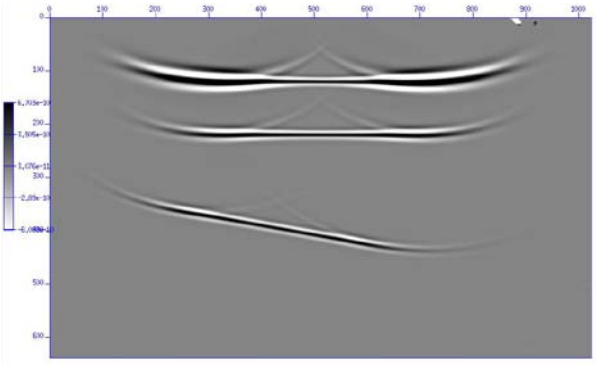

Figure 11 - RTM image for the directional wavefield propagator for the dipping reflector model.

One feature of the directional scheme in the migrated image for the dipping reflector is the smaller amplitude of the artifacts above the reflector. Therefore, it is expected that the reflection coefficient trend for this reflector will be less influenced by these artifacts than the coefficient obtained for the conventional case. Figure 12 shows the coefficient results for the dipping reflector.

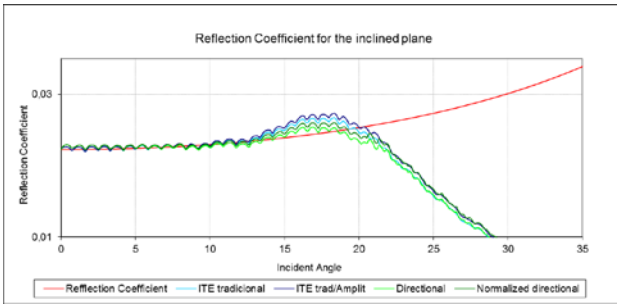

Figure 12 - Measured and theoretical reflection coefficient for the dipping reflector in the second model.

The results in Figure 12 can be seen in greater detail when the relative error of each calculated coefficient is plotted (Figure 13).

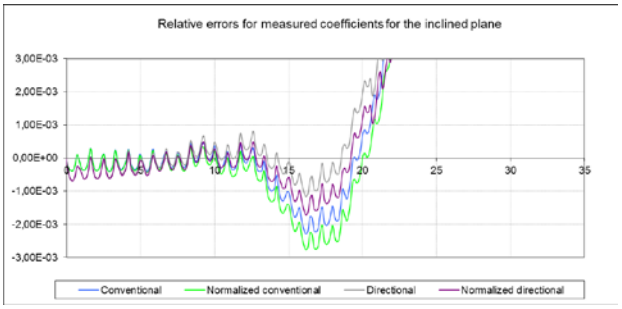

Figure 12 - Relative error for the reflection coefficient for the dipping reflector in the second model.

A periodic oscillation in the measured graphs is shown in figures 12 and 13. This is due to the discrete grid structure of the dipping reflector.

Conclusions

It is possible to obtain depth images from Reverse Time Migration in which the amplitude variation follows the trend of the theoretical reflection coefficient. This enables AVA and AVO analyses to be performed in depth images generated by RTM.

In the case of the excitation time imaging condition, the use of the amplitude matrix as a normalization factor resulted in an improvement of the depth image amplitude behavior as a function of the incident angle.

The application of the directional separation scheme didn't significantly improve the results in the studied models, where there are predominantly horizontal reflectors and low incident angles.

Acknowledgments

The authors would like to thank Petrobras for authorizing this publication.

References

Baysal, E., Kosloff, D. & Sherwood, J.W.C., 1984. A two-way nonreflecting wave equation. *Geophysics*, 49, 132-14.

Bulcão, A., Soares Filho, D.M. & Mansur, W.J., 2007. Improved Quality of Depth Images Using Reverse Time Migration. *SEG/San Antonio 2007 Annual Meeting*.

Chattopadhyay, S. & McMechan, G.A., 2008. Imaging conditions for prestack reverse-time migration. *Geophysics*, 73, S81-S89.

Levander, A.R., 1988. Fourth-order finite-difference P-SV seismograms. *Geophysics*, 53, no. 11, 1425.

Loewenthal, D. & Hu, L., 1991. Two methods for computing the imaging condition for common-shot prestack migration. *Geophysics*, 56, no. 3, 378.

Sava, P. & Hill, S.J., 2009. Overview and classification of wavefield seismic imaging methods. *The Leading Edge*, 28, no. 2, 170.

Silva, A.P.S., Bulcão, A. & Landau, L., 2010. Seismic image and AVA analyses using the reverse time migration (RTM) method with different wave equation implementations. *Proceedings of The International Workshop on Applied Modeling & Simulation*, Rio de Janeiro.

Zhang, Y., Sun, J. & Gray, S., 2007. Reverse-time migration: amplitude and implementation issues. *SEG/San Antonio 2007 Annual Meeting*.